

STEEDEITE, $\text{NaMn}_2[\text{Si}_3\text{BO}_9](\text{OH})_2$: CHARACTERIZATION, CRYSTAL-STRUCTURE DETERMINATION, AND ORIGIN

MONIKA M.M. HARING AND ANDREW M. MCDONALD[§]

Department of Earth Sciences, Laurentian University, Sudbury, Ontario P3E 2C6, Canada

ABSTRACT

Steedeite, ideally $\text{NaMn}_2\text{Si}_3\text{BO}_9(\text{OH})_2$, is a new mineral discovered in altered sodalite syenite at the Poudrette quarry, La Vallée-du-Richelieu, Montérégie (formerly Rouville County), Québec, Canada. Crystals of steedeite are colorless to pale pink, and acicular with average dimensions of $0.006 \times 0.011 \times 0.51$ mm. They occur as radiating to loose, randomly oriented groupings within vugs associated with aegirine, nepheline, sodalite, eudialyte-group minerals, analcime, natron, pyrrhotite, catapleite, and two other unidentified minerals temporarily designated UK78 and UK80. Steedeite is transparent to translucent with a vitreous luster and has a weak pale green to pale yellow fluorescence under medium-wave radiation. No partings or cleavages were observed, although crystals exhibit an uneven fracture. The calculated density is 3.106 g/cm^3 . Steedeite is nonpleochroic, biaxial with $n_{\text{min}} = 1.636(2)$ and $n_{\text{max}} = 1.656(2)$ and a positive elongation. Chemical analyses ($n = 14$) from seven crystals gave an average (range, standard deviation) of: Na_2O 7.51 (6.78–8.32, 0.44), CaO 0.17 (0.08–0.22, 0.03), MnO 31.02 (29.91–32.83, 0.93), FeO 0.86 (0.76–1.01, 0.07), SiO_2 46.34 (40.39–49.29, 2.56), S 0.39 (**b.d.*–2.36, 0.71) (**b.d.* = below detection), B_2O_3 (calc.) 8.73, and H_2O (calc.) 4.52, total 99.53 wt.%. The empirical formula is: $\text{Na}_{0.97}(\text{Mn}_{1.75}\text{Fe}_{0.05}\text{Ca}_{0.01})_{\Sigma 1.83}(\text{Si}_{3.07}\text{S}_{0.02})_{\Sigma 3.09}\text{BO}_9(\text{OH})_2$, or ideally $\text{NaMn}_2\text{Si}_3\text{BO}_9(\text{OH})_2$. The presence of both B and OH in steedeite were inferred from the refinement of the crystal structure. The Raman spectrum for steedeite show bands at $3250\text{--}3500 \text{ cm}^{-1}$ attributed to O–H stretching, strong sharp bands at $575\text{--}750 \text{ cm}^{-1}$ and $825\text{--}1075 \text{ cm}^{-1}$ attributed to Si–O bonds and possibly B–O bonding, as well as weak to strong bands at $50\text{--}500 \text{ cm}^{-1}$ attributed to Na–O/Mn–O bonds. Steedeite crystallizes in space group $P\bar{1}$ (#2) with a 6.837(1), b 7.575(2), c 8.841(2) Å, α 99.91(3), β 102.19, γ 102.78(3)°, V 424.81 Å³, and $Z = 2$. The strongest six lines on the X-ray powder-diffraction pattern [d in Å (1) (hkl)] are: 8.454 (100) (00 $\bar{1}$), 7.234 (39) (00 $\bar{1}$), 3.331 (83) ($1\bar{2}1$, $0\bar{1}\bar{2}$, $20\bar{1}$, $1\bar{1}\bar{2}$), 3.081 (38) ($0\bar{2}\bar{1}$), 2.859 (52) ($0\bar{1}\bar{3}$), and 2.823 (80) ($21\bar{1}$). The crystal structure of steedeite was refined to $R = 1.68\%$ and $wR_2 = 4.96\%$ for 2409 reflections ($F_o > 4\sigma F_o$). It is based on silicate chains with a periodicity of three (*i.e.*, dreier chain) consisting of four-membered borosilicate rings of composition $[\text{BSi}_3\text{O}_9(\text{OH})_2]^{5-}$. The borosilicate chains are classed as single loop-branched dreier chains that are linked together through shared corners to bands of edge-sharing $\text{MnO}_5(\text{OH})$ octahedra. Steedeite is a chain silicate mineral closely related to the sérandite–pectolite series of the pyroxenoid group and is the first mineral found to contain single loop-branched dreier silicate chains.

Keywords: steedeite, Mont Saint-Hilaire, crystal structure, borosilicate, sérandite – pectolite, loop-branched dreier chain, Raman spectrum

INTRODUCTION

Steedeite, ideally $\text{NaMn}_2\text{Si}_3\text{BO}_9(\text{OH})_2$, is a new borosilicate mineral from Mont Saint-Hilaire, Québec, Canada, one of the world's most prolific localities for new minerals (Chao *et al.* 1990). The mineral occurs as fine acicular crystals whose size initially prohibited the determination of its structure *via* standard four-circle diffractometers employing scintillation detectors. Collection of data required for determination of the crystal structure of steedeite has now been made possible, owing to recent advancements in single-crystal X-ray diffraction instrumentation including high-flux

sources and charge-coupled detectors of greater sensitivity. Determination and refinement of the crystal structure were critical not only to confirming the presence of both H_2O and (OH) in the mineral, but also in recognizing that the mineral contains essential B_2O_3 . In this contribution we present a complete crystal-chemical characterization of steedeite, elucidate the relationship of this mineral to members of the sérandite–pectolite series, and provide insights into the conditions that led to its formation. The mineral has been named for Mr. Anthony Hosford Steede (*b.* 1940) in recognition of his contributions to understanding the mineralogy of Mont Saint-Hilaire. Both the mineral and mineral name

[§] Corresponding author: amcdonald@laurentian.ca

have been approved by the International Mineralogical Association, Commission on New Minerals and Mineral Names (2013 – 052). The holotype material is housed in the collections of the Department of Natural History, Royal Ontario Museum (Toronto, Ontario, Canada), catalogue number M56489.

OCCURRENCE

Steedeite was discovered by Col. Quintin Wight in August 1987 and was temporarily designated UK79. The mineral was discovered in ~1 cm diameter vugs in a loose boulder (~1 × 1 m) of sodalite syenite at the Poudrette quarry, La Vallée-du-Richelieu, Montérégie (formerly Rouville County), Québec, Canada (45°33'8"N, 73°9'3"W). The loose boulder was found in the southeast portion of the quarry, in proximity to a large number of so-called sodalite syenite xenoliths (tawites) in nepheline syenite (McDonald & Chao 2010, 2005). The boulder containing steedeite was first noted owing to the abundance of relatively thick, euhedral plates of pyrrhotite contained within it. When the boulder was broken up, numerous centimeter-sized vugs

filled with clear, crystalline natron ($\text{Na}_2\text{CO}_3 \cdot 10\text{H}_2\text{O}$) or natrite (Na_2CO_3) were exposed, but these have subsequently decrepitated to thermonatrite ($\text{Na}_2\text{CO}_3 \cdot \text{H}_2\text{O}$) and related minerals. The sample containing steedeite consists predominantly of microcline, analcime, and nepheline along with aegirine and pyrrhotite (Table 1). The pyrrhotite associated with steedeite is magnetic, suggesting that it is the monoclinic 4C polytype. The rest of the sample is dominated by sodalite, a eudialyte-group mineral, sérandite, catapleite, and thermonatrite (Table 1). Some crystals of sodalite have been found to retain their violet color even after prolonged (*i.e.*, several years) exposure to the elements and sunlight. The sérandite is highly unusual for the locality in that it ranges in color from dark to pale green and brown to light brown, unlike the pink to orange coloration that typically characterizes the mineral. It may also be noteworthy that sérandite and steedeite have not been found together in the same vug, an interesting observation given their shared crystal chemistry. In addition, there are also two rare, unidentified minerals, tentatively referred to as UK78 and UK80 (Table 1). The unidentified minerals, like steedeite, also appear to be late-stage

TABLE 1. DESCRIPTION AND MODAL ABUNDANCES OF MINERALS OCCURRING WITH STEEDEITE

Mineral	Modal Abundance	Description
microcline (KAlSi_3O_8)	~68%	Aggregates of anhedral light grey crystals with a massive habit and greasy luster.
analcime $\text{Na}_2(\text{Al}_2\text{Si}_4\text{O}_{12}) \cdot 2\text{H}_2\text{O}$	~10%	Anhedral to subhedral translucent to transparent crystals with a vitreous luster.
nepheline ($\text{Na,K})\text{AlSiO}_4$	~7%	Anhedral, greenish-grey crystals with a greasy luster.
aegirine $\text{NaFe}^{3+}\text{Si}_2\text{O}_6$	~5%	Dark green, prismatic, euhedral crystals ranging in size from ~ 0.1 to 0.7 mm in length and dominated by the form prism {110}.
pyrrhotite Fe_{1-x}S	~5%	Pseudohexagonal crystals, ~ 4 mm in diameter, displaying the forms pinacoid {001}, pinacoid {100}, prism {100}, and prism {h0l}.
sodalite $\text{Na}_8(\text{Al}_6\text{Si}_6\text{O}_{24})\text{Cl}_2$	~2%	Anhedral, transparent crystals with a pale blue to violet color and a strong fluorescence under short-, medium-, and long-wave radiation.
eudialyte-group mineral $\text{Na}_{15}\text{Ca}_6(\text{Fe}^{2+}, \text{Mn}^{2+})_3\text{Zr}_3[\text{Si}_{25}\text{O}_{73}] (\text{O,OH,H}_2\text{O})_3(\text{OH,Cl})_2$	~1%	Euhedral, translucent to transparent crystals with a dark brown to orange color.
sérandite $\text{Na}(\text{Mn}^{2+}, \text{Ca})_2\text{Si}_3\text{O}_8(\text{OH})$	~1%	Radiating spheres composed of prismatic crystals with flattened terminations (pinacoid {001}). These crystals range in color from dark to pale green and brown to light brown.
thermonatrite $\text{Na}_2\text{CO}_3 \cdot \text{H}_2\text{O}$	~1%	White anhedral to subhedral, translucent crystals.
catapleite $(\text{Na,Ca},\square)_2\text{ZrSi}_3\text{O}_9 \cdot 2\text{H}_2\text{O}$	trace	Clear, colorless, pseudo hexagonal plates overgrowing sérandite.
UK78	trace	Clusters of radiating to randomly oriented, acicular, light green crystals with dimensions similar to those of steedeite.
UK80	trace	Flat clusters of radiating, brown crystals with dimensions similar to those of steedeite.

phases and it may be noteworthy that the three minerals have not been found together in the same vug.

PHYSICAL AND OPTICAL PROPERTIES

Crystals of steedeite are euhedral, acicular, and elongate along [001], and occur in slightly radiating to loose, randomly oriented groupings ('nests') (Fig. 1). They exhibit the forms pinacoid {100} (dominant), as well as the pinacoids {010} and {001} (minor). Crystals have average dimensions $0.006 \times 0.01 \times 0.5$ mm with average length-to-width ratios of ~46–85. They are pale pink to colorless with a white streak and a vitreous luster. Steedeite is unusual in that its crystals exhibit a weak pale green to pale yellow luminescence under medium-wave ultraviolet light. To date, the only other mineral from MSH apparently known to exhibit luminescence under medium-wave ultraviolet light is lalondeite, $(\text{Na,Ca})_6(\text{Ca,Na})_3\text{Si}_{16}\text{O}_{38}(\text{F,OH})_2 \cdot 3\text{H}_2\text{O}$ (McDonald & Chao 2009). Due to the small size of the crystals, a Mohs' hardness could not be measured. A density of 3.106 g/cm^3 was calculated using the empirical chemical formula and unit-cell parameters derived from the crystal-structure analysis.

A complete set of optical data for steedeite could not be collected due to the small crystal size and highly acicular nature of the mineral. Steedeite is assumed to be a biaxial, based on its symmetry. It exhibits a positive elongation and refractive indices of $n_{\min} = 1.636(2)$ and $n_{\max} = 1.656(2)$ as measured with a Na-vapor lamp ($\lambda = 589 \text{ nm}$). No pleochroism was observed. The Gladstone-Dale value, calculated using the empirical formula and unit-cell parameters derived from the crystal structure analysis, gives a compatibility index of 0.003 and is considered superior (Mandarino 1981).

CHEMICAL COMPOSITION

Chemical analyses of steedeite were collected using a JEOL JSM 6400 scanning electron microscope equipped with an energy dispersive spectrometer and operating conditions of: voltage = 20 kV, ~1 nA beam current, and ~1 μm beam width. Energy-dispersive data were collected using the following standards: albite ($\text{NaK}\alpha$), perovskite ($\text{CaK}\alpha$), tephroite ($\text{MnK}\alpha$, $\text{SiK}\alpha$), and chalcopyrite ($\text{FeK}\alpha$, $\text{SK}\alpha$). Analyses ($n = 14$) of seven crystals gave an average (range, standard deviation) of: Na_2O 7.51 (6.78–8.32, 0.44), CaO 0.17 (0.08–0.22, 0.03), MnO 31.02 (29.91–32.83, 0.93), FeO 0.86 (0.76–1.01, 0.07), SiO_2 46.34 (40.39–49.29, 2.56), S 0.39 (**b.d.*–2.36, 0.71) (**b.d.* = below detection), B_2O_3 (calc.) 8.73, and H_2O (calc.) 4.52, total 99.53 wt.%. The presence of elements including B and H were confirmed through a combination of crystal-structure and Raman analyses (see below), respectively. The empirical formula, based on 11 anions, is $\text{Na}_{0.97}(\text{Mn}_{1.75}\text{Fe}_{0.05}\text{Ca}_{0.01})_{\Sigma 1.83}(\text{Si}_{3.07}\text{S}_{0.02})_{\Sigma 3.09}\text{BO}_9(\text{OH})_2$, or ideally $\text{NaMn}_2\text{Si}_3\text{BO}_9(\text{OH})_2$. The ideal formula requires Na_2O 7.63,

MnO 34.95, SiO_2 44.40, B_2O_3 8.58, and H_2O 4.44 wt.%, total 100.00 wt.%. Steedeite does not effervesce in 10% HCl at room temperature. The lower than ideal sum for the Mn site may be the result of analytical error associated with the small sizes of the crystals being analyzed, as the crystal structure refinement for steedeite shows the Mn sites to be fully occupied.

RAMAN SPECTROSCOPY

A Raman spectrum of steedeite, based on an average of three 20 s acquisition cycles over a range of 50 to 4000 cm^{-1} , was collected using a Horiba Jobin Yvon XPLORA Raman spectrometer interfaced with an Olympus BX41 microscope. An excitation radiation of $\lambda = 638 \text{ nm}$ was used along with a 600 grating and 100 \times magnification (producing a beam of diameter ~2 μm). The excitation radiation of $\lambda = 638 \text{ nm}$ was chosen to minimize fluorescence peaks in the region of ~2000 to 2800 cm^{-1} that were observed when the mineral was analyzed using the more typically employed radiation of $\lambda = 532 \text{ nm}$. Calibration was done using the 521 cm^{-1} line of a silicon wafer. The Raman spectrum (Fig. 2) contains five absorption bands located at regions of: ~50–500 cm^{-1} , 575–750 cm^{-1} , 825–1075 cm^{-1} , 1500–2000 cm^{-1} , and 3250–3500 cm^{-1} . In the first region (~50–500 cm^{-1}) five weak to strong bands at 120, 197, 264, 330, and 431 cm^{-1} are present. Bands at 197, 264, 330, and 430 cm^{-1} are attributed to Mn–O bonding (Table 2), based on data from Julien *et al.* (2004) for manganese oxide minerals such as pyrolusite, ramsdellite, and birnessite. The bands at 330 and 430 cm^{-1} could not be unequivocally assigned due to overlap between lower frequency Mn–O and Na–O, Si–O–Si and Si–O–B bands, respectively (Julien *et al.* 2004, Williams 1995). In the second region (575–750 cm^{-1}), one very strong band at 636 cm^{-1} and a weaker band at 696 cm^{-1} are present. These are attributed to

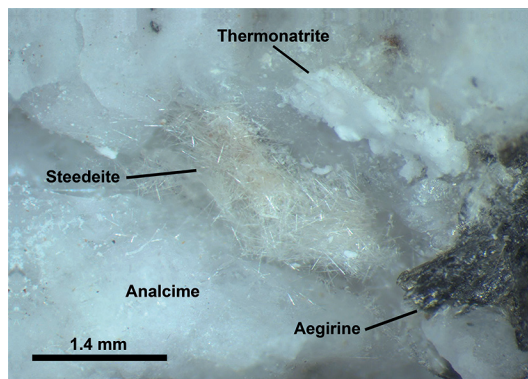


FIG. 1. Loose aggregates of steedeite with natron, aegirine, and analcime (FOV: 1.0 mm)

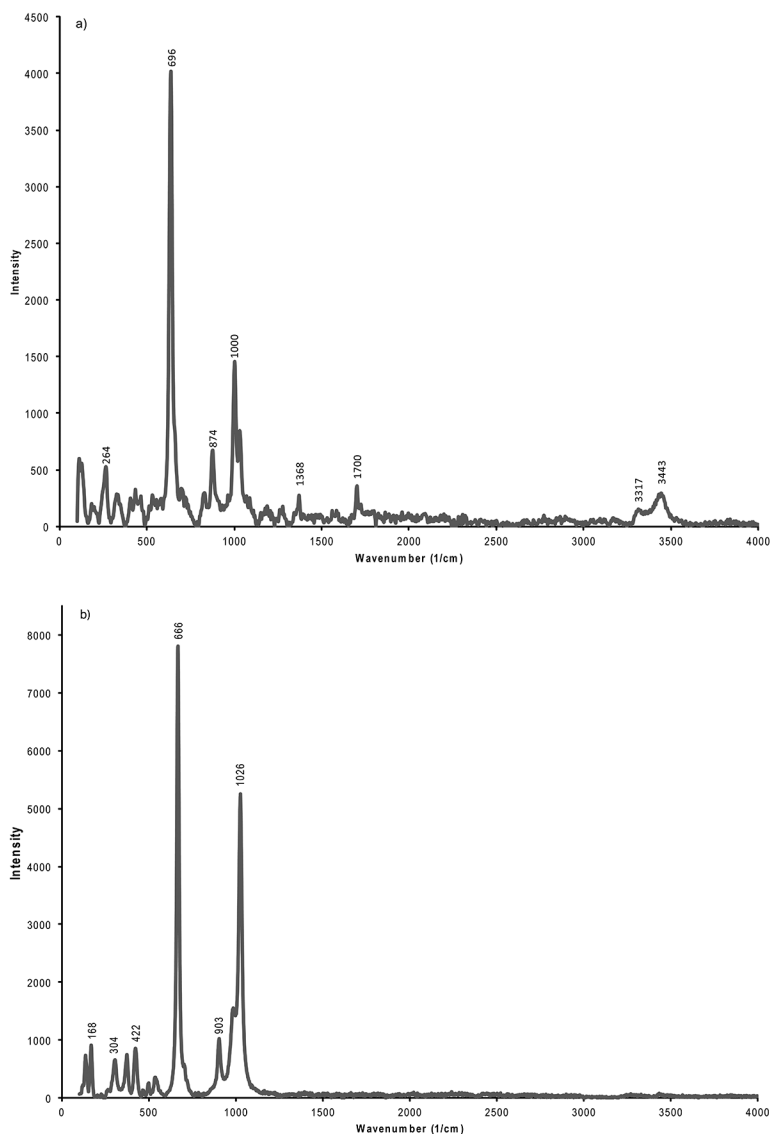


FIG. 2. Raman spectrum for (a) steedeite and (b) sérandite.

Si–O–Si and Si–O–B bending (Williams 1995, Frost *et al.* 2007), although there is potential for overlap as absorption peaks for Mn–O can occur at similar frequencies (Julien *et al.* 2004) (Table 2). The third region ($\sim 800\text{--}1075\text{ cm}^{-1}$) consists of four moderately strong bands at 826, 874, 1000, and 1030 cm^{-1} . The bands at 826 and 874 cm^{-1} are attributed to symmetric stretching of Si–O bonds and bands at 1000 and 1030 cm^{-1} to asymmetric stretching of Si–O bonds (Williams 1995; Table 2). Alternatively, the two bands at 1000 and 1030 cm^{-1} could also be attributed to B–O stretching

based on data from Frost *et al.* (2007) for ferroaxinite. Two additional bands at 1368 and 1700 cm^{-1} are attributed to C–O and H–O–H bonds, respectively (Williams 1995). As refinement of the crystal structure of steedeite indicates that neither CO_3 nor H_2O are present in the mineral, the additional bands are likely associated with the small amounts of thermonatrite that overgrow steedeite. The fifth region (~ 3250 and 3500 cm^{-1}) contains two moderately strong bands at 3317 and 3443 cm^{-1} , attributed to O–H bending (Williams 1995). Given the chemical and structural similarities between steedeite

and sérandite, a Raman spectrum of pink sérandite from MSH was also collected for the purpose of comparison (Fig. 2). Results indicate the two spectra are very similar, except that the Raman spectrum for steedeite contains additional weak to moderately strong bands at 826 and 874 cm^{-1} .

X-RAY CRYSTALLOGRAPHY AND CRYSTAL-STRUCTURE DETERMINATION

Powder X-ray diffraction data were collected using a 114.6 mm diameter Gandolfi camera, 0.3 mm collimator, and Fe-filtered $\text{CoK}\alpha$ radiation ($\lambda = 1.7902 \text{ \AA}$). Intensities were determined using a scanned image of the powder pattern normalized to the measured intensity of $d = 8.454 \text{ \AA}$ ($I = 100$). A theoretical powder pattern was calculated using the results from the crystal-structure analysis with the program CRYSCON (Dowty 2002) and is in good agreement with the measured powder pattern (Table 3).

X-ray intensity data were collected with a Bruker D8 three-circle diffractometer equipped with a rotating-

anode generator, multi-layer optics incident beam path, and an APEX-II CCD detector. An excess of a sphere of X-ray diffraction data (total of 15061 reflections) was collected to $60^\circ 2\theta$ using 20 s per 0.3° frame with a crystal-to-detector distance of 5 cm. The unit-cell parameters were obtained by least-squares refinement of 14135 reflections ($I > 10\sigma I$), and are given in Table 4. Empirical absorption corrections (SADABS; Sheldrick 1998) were applied and identical data merged to give 15014 reflections covering the entire Ewald sphere. Information pertaining to the data collection is given in Table 4.

Solution and refinement of the crystal structure of steedeite were done using SHELXL – 97 (Sheldrick 2008, 1997). The crystal structure was solved by direct methods, using the scattering curves of Cromer & Mann (1968) and the scattering factors of Cromer & Liberman (1970). Phasing of a set of normalized structure factors gave the mean $|E^2 - 1|$ value of 0.996, consistent with a centrosymmetric space group. In light of this and the absence of systematic extinctions, $P1$ was selected as the correct space group. Phase-normalized structure

TABLE 2. OBSERVED ABSORPTION BANDS AND BAND ASSIGNMENTS FOR THE RAMAN SPECTRUM OF STEEDEITE.

Raman Absorption Bands for steedeite (cm^{-1})	Raman Absorption Bands for sérandite (cm^{-1})	Suggested Assignment
3443		O–H Stretching
3317		O–H Stretching
1700		H–O–H bending
1368		C–O bending
1030	1026	Asymmetric stretching mode of Si–O _{nbr} / B–O stretching
1000		Asymmetric stretching mode of Si–O _{nbr} / B–O stretching
	984	Asymmetric stretching mode of Si–O _{nbr} / B–O stretching
	903	Asymmetric stretching mode of Si–O _{nbr} / B–O stretching
874		Symmetric stretching mode of Si–O _{br}
826		Symmetric stretching mode of Si–O _{br}
696	703	Si–O–Si and Si–O–B Bending/ Mn–O
	666	Si–O–Si and Si–O–B Bending/ Mn–O
636		Si–O–Si and Si–O–B Bending/ Mn–O
	535	Si–O–Si and Si–O–B Bending/ Mn–O
	497	Si–O–Si and Si–O–B Bending/ Mn–O
	466	Si–O–Si and Si–O–B Bending/ Mn–O
431	422	Si–O–Si and Si–O–B Bending/ Mn–O
	373	Si–O–Si and Si–O–B Bending/ Mn–O
330		Si–O–Si Bending/ O–Si–O Bending/ Mn–O
	304	Mn–O
264		Mn–O
197		Mn–O
	168	Mn–O/ Na–O
	134	Mn–O/ Na–O
120		Na–O

TABLE 3. STEEDEITE X-RAY POWDER DIFFRACTION DATA

l_{meas}	l_{calc}	$d_{\text{meas}} \text{ \AA}$	$d_{\text{calc}} \text{ \AA}$	h	k	l
100	100	8.454	8.411	0	0	$\bar{1}$
39	30	7.234	7.190	0	$\bar{1}$	0
18	13	6.243	6.215	0	$\bar{1}$	1
8	3	4.240	4.264	1	1	0
	4		4.205	0	0	$\bar{2}$
6	6	4.083	4.059	0	$\bar{1}$	2
19	2	3.619	3.620	0	$\bar{2}$	1
	10		3.599	1	1	$\bar{2}$
83	9	3.331	3.392	1	$\bar{2}$	1
	52		3.314	0	$\bar{1}$	$\bar{2}$
	2		3.307	2	0	$\bar{1}$
	17		3.289	1	$\bar{1}$	$\bar{2}$
38	25	3.081	3.062	0	$\bar{2}$	$\bar{1}$
11	9	2.979	2.962	1	2	$\bar{1}$
52	27	2.859	2.842	0	$\bar{1}$	3
80	71	2.823	2.814	2	$\bar{1}$	$\bar{1}$
18	14	2.525	2.508	0	$\bar{2}$	3
21	13	2.477	2.459	0	$\bar{3}$	1
8	9	2.336	2.324	0	$\bar{3}$	2
12	11	2.248	2.237	2	2	$\bar{1}$
	10		2.229	2	$\bar{3}$	0
25	17	2.169	2.156	0	$\bar{1}$	4
4	7	2.118	2.103	0	0	$\bar{4}$
2	2	2.083	2.072	0	$\bar{3}$	3
6	5	1.948	1.943	2	$\bar{3}$	$\bar{2}$
5	3	1.913	1.915	2	$\bar{1}$	$\bar{4}$
3	3	1.729	1.720	2	$\bar{2}$	4
7	20	1.691	1.709	4	$\bar{1}$	$\bar{1}$
6	6	1.598	1.596	2	4	$\bar{2}$
4	1	1.482	1.488	4	1	0
	2		1.481	2	4	$\bar{2}$

TABLE 4. MISCELLANEOUS SINGLE CRYSTAL DATA FOR STEEDEITE

a (Å)	6.837(1)	Monochromator	Graphite
b	7.575(2)	Intensity-data collection	0:20
c	8.841(2)	Criterion for observed	
α (°)	99.91(3)	reflections	$F_o > 4\sigma(F_o)$
β	102.19(3)	GooF	0.953
γ	102.78(3)	total No. of reflections collected	15061
V (Å ³)	424.81(1)	No. Unique reflections	2487
Space group	$P\bar{1}$ (#2)	No. Observed reflections	2409
Z	2	R (merge %)	1.71
D_{calc} (g/cm ⁻³)	3.106	R %	1.68
Radiation	MoK α (50 kV, 40 mA)	wR_2 %	4.96

factors were used to give a difference Fourier map from which one *Na*, three *Si*, two *Mn*, and several *O* sites were located. From subsequent difference-Fourier maps, a [4]-coordinated site was located with bond distances ranging from 1.467 to 1.509 Å, consistent with B–O bond lengths observed in other minerals (e.g., vistepite [SnMn₄B₂Si₄O₁₆(OH)₂; Hybler *et al.* 1997], bobtrillite [(Na,Ca)₁₃Si₁₁(Zr,Y,Nb)₁₄Si₄₂B₆O₁₃₂

(OH)₁₂•12H₂O; McDonald & Chao 2005], and reedmergnerite (NaBSi₃O₈; Appleman & Clark 1965); on this basis, the site was assigned to B. Refinement of the site-occupancy factors (SOF) indicated that all of cation and anion sites are fully occupied, a point particularly relevant when discussing the nature of Si–B ordering in steedeite (Table 5). Determination of which *O* sites were occupied by OH was based on bond-valence

calculations and electroneutrality considerations (Table 7). At the later stages of refinement, two *H* sites were located in the difference Fourier maps. These H sites were inserted into the refinement and the H–O distances were constrained to be close to 0.98 Å. Refinement of this model converged to $R = 1.68\%$ and $wR_2 = 4.96\%$ for 2409 reflections ($F_o > 4\sigma F_o$).

CRYSTAL STRUCTURE

Cation Polyhedra

The crystal structure of steedeite contains three *Si* sites, two *Mn* sites, and one unique site each for *Na* and *B* (Table 5). The three *Si* sites are coordinated by four crystallographically distinct O atoms with Si–O bond lengths ranging from 1.602(1) to 1.657(1) Å (Table 6; Jacobsen *et al.* 2000). The B site is coordinated by two O atoms and two (OH) groups, forming BO₂(OH)₂ tetrahedra with B–(O,OH) bond lengths ranging from 1.467(2) to 1.508(2) Å, where both the shortest and longest bond distances correspond to B–OH bonds (Table 6). The BO₂(OH)₂ tetrahedra has also been found in the synthetic phases Pb₆B₁₁O₁₈(OH)₉ (Villars *et al.* 2010) and (Mn,Fe,Co)²⁺[BPO₄(OH)₂] (Huang *et al.* 2006). This type of B–O tetrahedron is extremely unusual, having only been reported in one other mineral: rogermitchellite [Na₁₂(Sr,Na)₂₄Ba₄Zr₂₆Si₇₈(B,Si)₁₂O₂₄₆(OH)₂₄•18H₂O; McDonald & Chao 2010], which also occurs at Mont Saint-Hilaire. At the same time, preliminary results from refinement of the crystal structure of UK 78 (Haring *et al.* in prep) suggest that a similar B–O tetrahedron may also be present in this mineral.

The variation observed in the B–(O,OH) bond lengths in steedeite falls within the typical range of 1.462 to 1.512 Å observed for ¹⁴B in other borosilicate minerals (Hawthorne *et al.* 1996). Based on radii from Shannon (1976), the ideal B–(O,OH) bond length for tetrahedral B is 1.477 Å (Hawthorne *et al.* 1996) and as the average <B–(O,OH)> bond length of 1.479 Å for steedeite falls within < 1% of this value, the site appears to be only occupied by B (*i.e.*, the mineral is strongly ordered with respect to B). In combination with the observed Si–O bond distances, the structural data clearly indicate that Si and B are ordered in steedeite.

The two *Mn* sites are coordinated by five O atoms, and one (OH) group, forming MnO₅(OH) octahedra. These octahedra have Mn–(O,OH) bond lengths ranging from 2.153(1) to 2.356(1) Å (Table 6), similar to Mn–(O,OH) bond distances observed in sérandite (Jacobsen *et al.* 2000). The bond-valence-sums for both Mn sites are close to 2+ (Table 7). Furthermore, the average <Mn–(O,OH)> bond lengths are 2.233 and 2.208 Å for the Mn(1)O₅(OH) and Mn(2)O₅(OH) octahedra, respectively. This corresponds to atomic radii of 0.87 and 0.85 Å, respectively, for Mn(1) and Mn(2) if the ionic radii for O/OH is assumed to be 1.36 Å based on an average O/OH coordination of 3.17 (Shannon 1976). These atomic radii for Mn(1) and Mn(2) are close to the ideal radius of 0.83 Å for Mn²⁺ in [6]-coordination (Shannon 1976), suggesting that Mn in steedeite is largely Mn²⁺. The *Na* site is coordinated with five O atoms and two (OH) groups, forming NaO₅(OH)₂ polyhedra, with Na–(O,OH) bond lengths ranging from 2.342(1) to 2.695(2) Å (<Na–(O,OH)> = 2.481 Å, Table 5). Unlike steedeite, the *Na* site in sérandite is coordinated by six O

TABLE 5. POSITIONAL AND DISPLACEMENT PARAMETERS FOR STEEDEITE

ATOM	<i>x</i>	<i>y</i>	<i>z</i>	<i>U</i> _{eq}	<i>U</i> ₁₁	<i>U</i> ₂₂	<i>U</i> ₃₃	<i>U</i> ₂₃	<i>U</i> ₁₃	<i>U</i> ₁₂
Na	–0.1247(1)	0.64118(9)	0.81008(7)	0.0199(1)	0.0315(3)	0.0176(3)	0.0158(3)	0.0050(2)	0.0101(3)	0.0123(3)
Mn1	0.12800(3)	0.87518(3)	0.60727(2)	0.00946(6)	0.0091(1)	0.0101(1)	0.0085(1)	0.00136(7)	0.00180(7)	0.00222(7)
Mn2	–0.38639(3)	0.86495(3)	0.59872(2)	0.01037(6)	0.0100(1)	0.0098(1)	0.0104(1)	0.00088(7)	0.00130(7)	0.00331(7)
Si1	–0.27055(5)	0.52647(5)	0.38313(4)	0.0076(1)	0.0076(2)	0.0062(2)	0.0083(2)	0.0008(1)	0.0018(1)	0.0016(1)
Si2	–0.53952(5)	0.74187(5)	0.21311(4)	0.0080(1)	0.0062(2)	0.0078(2)	0.0090(2)	0.0001(1)	0.0012(1)	0.0018(1)
Si3	0.01582(5)	0.73835(5)	0.22546(4)	0.0071(1)	0.0065(2)	0.0076(2)	0.0066(2)	0.0007(1)	0.0015(1)	0.0018(1)
B	–0.2798(2)	0.8757(2)	0.0291(2)	0.0057(2)	0.0043(5)	0.0074(5)	0.0046(5)	–0.0011(4)	0.0008(4)	0.0020(4)
O1	0.4415(1)	1.0798(1)	0.6388(1)	0.0101(2)	0.0103(4)	0.0086(4)	0.0095(4)	0.0000(3)	0.0012(3)	0.0017(3)
O2	–0.1887(2)	0.6853(1)	0.5474(1)	0.0104(2)	0.0110(4)	0.0090(4)	0.0099(4)	0.0003(3)	0.0023(3)	0.0021(3)
O3	–0.4806(2)	0.7830(1)	0.0524(1)	0.0140(2)	0.0111(4)	0.0160(5)	0.0128(4)	–0.0005(3)	0.0053(3)	0.0004(3)
O4	0.0839(2)	0.9205(1)	0.3686(1)	0.0101(2)	0.0119(4)	0.0088(4)	0.0085(4)	0.0002(3)	0.0021(3)	0.0022(3)
O5	–0.1274(2)	0.7708(1)	0.0698(1)	0.0135(2)	0.0144(4)	0.0162(4)	0.0097(4)	0.0009(3)	–0.0005(3)	0.0087(4)
O6	0.3217(1)	0.6841(1)	0.5976(1)	0.0110(2)	0.0100(4)	0.0080(4)	0.0155(4)	0.0034(3)	0.0042(3)	0.0021(3)
O7	–0.0939(2)	0.5540(1)	0.2805(1)	0.0117(2)	0.0133(4)	0.0095(4)	0.0136(4)	0.0028(3)	0.0072(3)	0.0022(3)
O8	–0.7925(1)	0.6785(1)	0.1678(1)	0.0109(2)	0.0067(4)	0.0125(4)	0.0124(4)	0.0000(3)	0.0024(3)	0.0028(3)
O9	–0.4764(2)	0.5622(1)	0.2688(1)	0.0133(2)	0.0116(4)	0.0095(4)	0.0161(4)	0.0011(3)	–0.0022(3)	0.0041(3)
OH10	0.1985(2)	0.9290(1)	0.8689(1)	0.0127(2)	0.0134(4)	0.0118(4)	0.0123(4)	0.0021(3)	0.0020(3)	0.0037(3)
OH11	–0.3053(2)	0.8805(2)	0.8609(1)	0.0244(3)	0.0424(7)	0.0320(6)	0.0092(4)	0.0084(4)	0.0091(5)	0.0259(6)
H1	0.287(3)	0.855(3)	0.914(3)	0.053(8)						
H2	–0.417(9)	0.766(7)	0.84(1)	0.39(6)						

TABLE 6. INTERATOMIC DISTANCES (Å) IN STEEDEITE

<i>NaO₆(OH)₂ Polyhedron</i>			<i>Si(1)O₄ Tetrahedron</i>		
<i>Na-O5</i>	2.342(1)		<i>Si1-O6</i>	1.602(1)	
<i>-O2</i>	2.367(1)		<i>-O2</i>	1.621(1)	
<i>-O8</i>	2.414(1)		<i>-O9</i>	1.654(1)	
<i>-OH11</i>	2.441(1)		<i>-O7</i>	<u>1.657(1)</u>	
<i>-O7</i>	2.477(1)		< <i>Si1-O</i> >	1.634 s.u.	
<i>-OH10</i>	2.627(2)				
<i>-O9</i>	<u>2.695(2)</u>		<i>Si(2)O₄ Tetrahedron</i>		
< <i>Na-O</i> >	2.481 s.u.		<i>Si2-O1</i>	1.615(1)	
			<i>-O3</i>	1.618(1)	
<i>Mn(1)O₅(OH) Octahedron</i>			<i>-O8</i>	1.630(1)	
<i>Mn1-O4</i>	2.165(1)		<i>-O9</i>	<u>1.638(1)</u>	
<i>-O6</i>	2.171(1)		< <i>Si2-O</i> >	1.625 s.u.	
<i>-OH10</i>	2.205(1)				
<i>-O2</i>	2.216(1)		<i>Si(3)O₄ Tetrahedron</i>		
<i>-O1</i>	2.281(1)		<i>Si3-O5</i>	1.602(1)	
<i>-O4</i>	<u>2.356(1)</u>		<i>-O4</i>	1.608(1)	
< <i>Mn1-O</i> >	2.233 s.u.		<i>-O8</i>	1.627(1)	
			<i>-O7</i>	<u>1.635(1)</u>	
<i>Mn(2)O₅(OH) Octahedron</i>			< <i>Si3-O</i> >	1.618 s.u.	
<i>Mn2-O6</i>	2.153(1)		<i>BO₂(OH)₂ Tetrahedron</i>		
<i>-O2</i>	2.178(1)		<i>B-O5</i>	1.468(2)	
<i>-O1</i>	2.183(1)		<i>-O3</i>	1.470(2)	
<i>-O1</i>	2.233(1)		<i>-OH11</i>	1.467(2)	
<i>-OH11</i>	2.243(1)		<i>-OH10</i>	<u>1.508(2)</u>	
<i>-O4</i>	<u>2.259(1)</u>		< <i>B-O</i> >	1.479 s.u.	
< <i>Mn2-O</i> >	2.208 s.u.				
Hydrogen Bonding					
<i>Donor-H</i>	<i>d(D-H; Å)</i>	<i>d(H...A; Å)</i>	< <i>DHA</i> (°)	<i>d(D...A; Å)</i>	<i>Acceptor</i>
OH10-H1	0.980	2.029	161.83	2.976	O3
OH11-H2	0.987	2.384	116.51	2.960	O6

TABLE 7. BOND-VALENCE TABLE (*v.u.*) FOR STEEDEITE

	Na	Mn(1)	Mn(2)	Si(1)	Si(2)	Si(3)	B	Σ	H(1)	H(2)	Σ
O1		0.265 ^{1→}	0.648 ^{1→}		1.025 ^{1→}			1.938			1.938
O2	0.216 ^{1→}	0.316 ^{1→}	0.350 ^{1→}	1.008 ^{1→}				1.890			1.890
O3					1.016 ^{1→}		0.765 ^{1→}	1.781	0.12 ^{1→}		1.901
O4		0.580 ^{1→}	0.282 ^{1→}			1.044 ^{1→}		1.906			1.906
O5	0.231 ^{1→}					1.061 ^{1→}	0.769 ^{1→}	2.061			2.061
O6		0.357 ^{1→}	0.375 ^{1→}	1.061 ^{1→}				1.793		0.08 ^{1→}	1.873
O7	0.160 ^{1→}			0.915 ^{1→}		0.971 ^{1→}		2.046			2.046
O8	0.190 ^{1→}				0.984 ^{1→}	0.992 ^{1→}		2.166			2.166
O9	0.089 ^{1→}			0.922 ^{1→}	0.963 ^{1→}			1.974			1.974
OH10	0.107 ^{1→}	0.326 ^{1→}					0.691 ^{1→}	1.124	0.88 ^{1→}		2.004
OH11	0.177 ^{1→}		0.294 ^{1→}				0.771 ^{1→}	1.242		0.92 ^{1→}	2.162
Σ	1.170	1.844	1.949	3.906	3.988	4.068	2.996		1.00	1.00	

* Bond valences for H sites determined using parameters from Brown & Altermatt (1985). Bond valences for other sites determined using parameters from Brese & O'Keeffe (1991).

atoms and two (OH) groups, resulting in a $\text{NaO}_6(\text{OH})_2$ polyhedron with a slightly larger $\langle \text{Na}-(\text{O},\text{OH}) \rangle$ bond length of 2.497 Å (Jacobsen *et al.* 2000).

Bond Topology

Each SiO_4 tetrahedron in the crystal structure of steedeite is linked to two adjacent SiO_4 tetrahedra through shared corners forming infinite single silicate chains parallel to *a* (*i.e.*, the elongation of steedeite crystals). The silicate chains have a repeat unit consisting of three symmetrically independent SiO_4 tetrahedra: $\text{Si}(1)\text{O}_4$, $\text{Si}(2)\text{O}_4$, and $\text{Si}(3)\text{O}_4$, forming C-shaped clusters (Fig. 3). The C-shaped clusters are closed by $\text{BO}_2(\text{OH})_2$ tetrahedra via shared corners, generating four-membered $[\text{BSi}_3\text{O}_{12}]^{7-}$ rings (Fig. 3). The $\text{BO}_2(\text{OH})_2$ tetrahedra are therefore considered to be the branching tetrahedra, so the silicate chain in steedeite can be classed as a loop-branched *dreier* chain silicate (Liebau 1978). The loop-branched tetrahedral chains are linked through shared corners to double chains of edge-sharing $\text{MnO}_5(\text{OH})$ octahedra. The resulting framework contains channels along $\{011\}$ that are occupied by Na (Fig. 4). The loop-branched silicate chains and $\text{MnO}_5(\text{OH})$ bands form distinct tetrahedral (*T*) and octahedral (*O*) layers, respectively, resulting in *T–O–T–O...* stacking perpendicular to $\{011\}$ (Fig. 4). The stacking pattern along with the linkages between the layers of tetrahedra and octahedra give rise to an I-beam topology (Thompson 1970) where bands of octahedra are linked to overlying and underlying silicate chains through the apical O atoms in the SiO_4 tetrahedra. In the crystal structure of steedeite these apical O atoms include O(7), O(5), O(2), and O(1) from the SiO_4 tetrahedra, as well as OH(11) and OH(10) from the $\text{BO}_2(\text{OH})_2$ tetrahedra.

Hydrogen Bonding

The structure of steedeite contains two (OH) groups, OH(10) and OH(11). The H(1) atoms, bonded to OH(10) groups, project towards adjacent borosilicate chains in the tetrahedral layer (Fig. 5). Each H(1) atom is located ~ 2.03 Å (Table 6) from O(3) atoms in adjacent borosilicate chains, such that each borosilicate chain within the tetrahedral layer is linked to adjacent chains through hydrogen bonding. The H(2) atoms, bonded to OH(11) groups, project towards borosilicate chains within adjacent tetrahedral sheets (Fig. 5). Each H(2) atom is located ~ 2.38 Å from O(6) atoms (Table 6) bonded to borosilicate chains, such that the tetrahedral layers are linked in part by hydrogen bonds along $\{011\}$.

RELATED STRUCTURES

The I-beam topology and the *T–O–T* stacking pattern present in steedeite are similar to that found

in other chain silicate minerals, specifically pyroxenoids of the pectolite ($\text{NaCa}_2[\text{Si}_3\text{O}_8\text{OH}]$)–sérandite ($\text{NaMn}_2[\text{Si}_3\text{O}_8\text{OH}]$) series, which are also hydrated and have *P* symmetry. The crystal structures of these minerals consist of *dreier* silicate chains (Waldemar 1955, Prewitt 1967) similar to those in steedeite, but they differ in that they are unbranched *dreier* chains, compared to the branched tetrahedral chains in steedeite (Fig. 4). Although the silicate chains in pectolite–sérandite are unbranched, they contain O...H–O groups (Arakcheeva *et al.* 2007), which fulfill the topological role of the $\text{BO}_2(\text{OH})_2$ tetrahedra in steedeite. Both steedeite and members of the pectolite–sérandite series contain double chains of edge-sharing octahedra. Steedeite is most closely related to sérandite in terms of its chemistry and crystal structure. Chemically, steedeite has proportions of Na, Mn, and Si identical to those of sérandite, but steedeite also possesses the $\text{BO}_2(\text{OH})_2$ group and an additional OH group.

The crystal structure of steedeite is also similar to that of scheuchzerite ($\{\text{Na}(\text{Mn},\text{Mg})_9[\text{VSi}_9\text{O}_{28}(\text{OH})](\text{OH})_3\}$; Brugger *et al.* 2006). Both minerals have hydrated loop-branched chain silicate structures, but the silicate chains in scheuchzerite are more complex, with a periodicity of seven and six-membered silicate rings that alternate with C-shaped silicate clusters similar to those that make up the repeating unit in steedeite (Brugger *et al.* 2006; Fig. 4). Each six-membered silicate ring within the silicate chain in scheuchzerite is linked through a shared corner to a single vanadate tetrahedron (VO_4)^{3–} (Brugger *et al.* 2006). The (VO_4)^{3–} group is considered to be a branching tetrahedron, therefore the silicate chain in scheuchzerite can be considered as being both loop-branched and open branched (Liebau 1978). The crystal structures of scheuchzerite and steedeite both contain bands of edge sharing $\text{Mn}(\text{O},\text{OH})_6$ octahedra. The bands of $\text{Mn}(\text{O},\text{OH})_6$ octahedra in scheuchzerite (Brugger *et al.* 2006) are wider than those in steedeite, with a single octahedral band varying from three to four octahedra wide, while that in steedeite is only two octahedra wide.

Loop-branched *dreier* chains such as those in steedeite are relatively uncommon, but similar chains can be found in charoite $[(\text{K},\text{Sr},\text{Ba},\text{Mn})_{15-16}(\text{Ca},\text{Na})_{32}[(\text{Si}_{70}(\text{O},\text{OH})_{180})](\text{OH},\text{F})_4 \cdot n\text{H}_2\text{O}]$. Here, the loop-branched *dreier* chains link with one another to form tubular *dreier* triple chains (Rozhdstvenskaya *et al.* 2010). The crystal structure of vlasovite $[\text{Na}_2\text{Zr}(\text{Si}_4\text{O}_{11})]$ (Sokolova *et al.* 2006) also contains silicate chains similar to those observed in steedeite, but with four-membered $[\text{Si}_4\text{O}_{11}]^{5-}$ rings that are inclined with respect to one another, such that the silicate chain has a repeating unit of six instead of three (Sokolova *et al.* 2006, Voronkov & Pyatenko 1962). Unlike steedeite, the crystal structure of vlasovite is a mixed zeolite-like framework where four loop-branched silicate chains are linked through shared corners to ZrO_6 octahedra

(Gobechiya *et al.* 2003). There are also two synthetic phases, $\text{Li}_2\text{Mg}_2(\text{Si}_4\text{O}_{11})$ (Maresch & Czank 1985, Czank & Bissert 1993) and $\text{Fe}_3\text{Be}(\text{Si}_3\text{O}_9)(\text{F},\text{OH})_2$ (Bakakin & Solov'eva 1971) that have single loop-branched *dreier* chains similar to those in steedeite. The crystal structure of $\text{Li}_2\text{Mg}_2(\text{Si}_4\text{O}_{11})$, as in steedeite, has tetrahedral chains consisting of C-shaped clusters of three SiO_4 tetrahedra. These clusters are closed by a fourth SiO_4 tetrahedron, instead of a $\text{BO}_2(\text{OH})_2$ tetrahedron as in steedeite, generating four-membered $(\text{Si}_4\text{O}_{11})^{6-}$ rings (Czank & Bissert 1993; Fig. 4). The silicate chains are linked through shared corners to double chains or bands of edge-sharing MgO_6 octahedra (Czank & Bissert 1993). The crystal structure of $\text{Fe}_3\text{Be}(\text{Si}_3\text{O}_9)(\text{F},\text{OH})_2$ contains loop-branched *dreier* silicate chains similar to those in steedeite, but with BeO_4 tetrahedra instead of $\text{BO}_2(\text{OH})_2$ tetrahedra closing the C-shaped silicate clusters. The silicate chains in $\text{Fe}_3\text{Be}(\text{Si}_3\text{O}_9)(\text{F},\text{OH})_2$ are linked through shared corners to triple chains of edge-sharing FeO_6 octahedra.

Four-membered borosilicate rings similar to those in steedeite can also be found in the crystal structure of reedmergnerite (NaBSi_3O_8 ; Appleman & Clark 1965) with the latter containing two SiO_4 and two BO_4 tetrahedra. These four-membered rings are linked through shared corners to adjacent rings in three dimensions, generating a framework structure, rather than the chain structure found in steedeite. Given the relationship between steedeite and reedmergnerite, the silicate chains in steedeite represent a degree of polymerization intermediate between chain silicate structures and framework structures.

RELATIONSHIP OF STEEDEITE TO BOROSILICATE MINERALS

Similar to silicate minerals, B-bearing minerals may be classified based on the degree of polymerization observed in $\text{B}(\text{O},\text{OH})_4$ tetrahedra. Hawthorne (1983) proposed a classification scheme based on the polymerization of polyhedra with high bond valences (*i.e.*, borate polyhedra and silicate tetrahedra). Within this classification scheme, possible polyhedral clusters include: (1) unconnected polyhedra, (2) finite clusters, (3) infinite chains, (4) infinite sheets, and (5) infinite frameworks (Hawthorne 1983). From the perspective of borate polyhedra, borosilicate minerals may be classified as those with crystal structures based on unconnected borate polyhedra (*e.g.*, ferroaxinite, tourmaline, and reedmergnerite) or those with crystal structures based on finite clusters of borate polyhedra (*e.g.*, tadjhikite, hellandite, danburite, and howlite; Hawthorne *et al.* 1996). Considering this, the crystal structure of steedeite is classified as being based on unconnected BO_4 tetrahedra similar to reedmergnerite and ferroaxinite.

There are ~100 known borosilicate minerals (excluding the tourmaline group) of which ~10 are known to be disordered with respect to Si and B. Since it is clear that the majority of borosilicates show a strong preference for Si–B ordering, it is perhaps not surprising that steedeite does as well. In Si–B ordering experiments conducted on reedmergnerite in the range of 400–500 °C, results indicated that those of longer duration (*i.e.*, >200 hours) promoted higher degrees

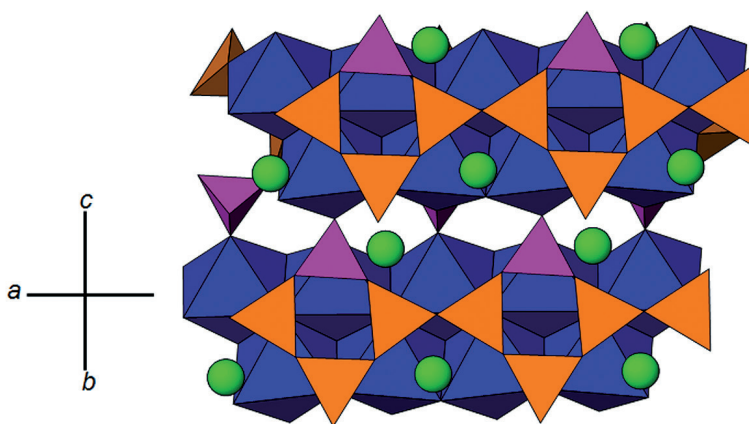


FIG. 3. The crystal structure of steedeite projected on to [011]. Both the bands of $\text{MnO}_5(\text{OH})$ and the loop-branched *dreier* chains run parallel to *a*. The Na atoms are green, SiO_4 tetrahedra are orange, $\text{BO}_2(\text{OH})_2$ tetrahedra are pink, and the $\text{MnO}_5(\text{OH})$ octahedra are blue.

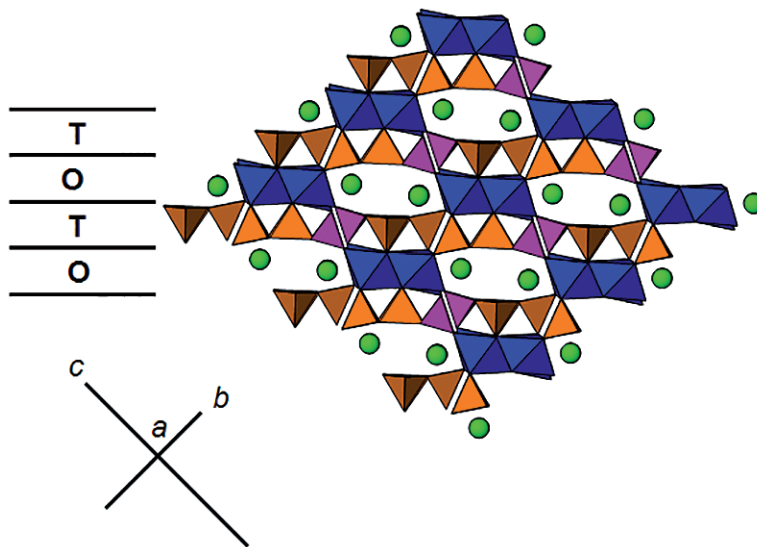


FIG. 4. The crystal structure of steedeite, projected onto [100], with tetrahedral (T) and octahedral (O) layers alternating perpendicular to [011]. The Na atoms are green, SiO_4 tetrahedra are orange, $\text{BO}_2(\text{OH})_2$ tetrahedra are pink, and the $\text{MnO}_5(\text{OH})$ octahedra are blue.

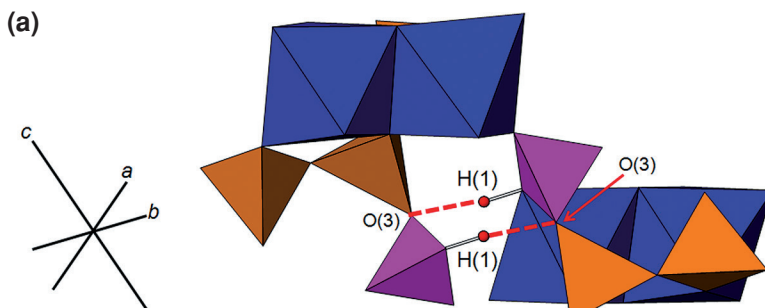
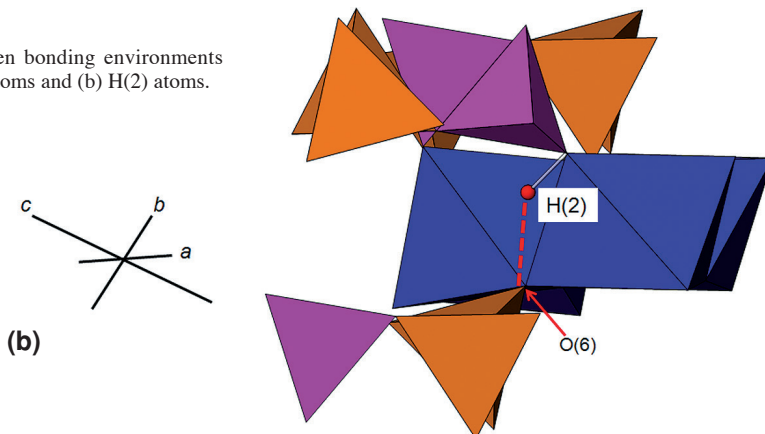


FIG. 5. Hydrogen bonding environments for (a) H(1) atoms and (b) H(2) atoms.



of Si–B ordering (Mason 1980). This suggests that steedeite crystals, which show a high degree of Si–B ordering, could have cooled over a protracted period of time. The experiments of Mason (1980) also showed Si–B disordered phases were found to be unstable relative to the Si–B ordered phases, the former exhibiting etching features which are evidence of dissolution (Mason 1980). The relative stability of Si–B ordered phases over Si–B disordered phases could thus explain the paucity of disordered borosilicates.

ORIGIN

Paragenetically, steedeite, along with sérandite, UK78, UK80, and thermonatrite, are late-stage phases which overgrow earlier-formed phases such as microcline, aegirine, and analcime (Table 8). Thermonatrite is inferred to have been the latest crystallizing phase, as it overgrows crystals of steedeite. The sequence of formation for steedeite, sérandite, UK78, and UK80 is unclear (Table 8), as none of these phases have been found together in the same vug.

The hydrous structure of steedeite and its occurrence in vugs suggests that it precipitated from late-stage aqueous fluids. These fluids are inferred to have been highly alkaline due to the presence of late-stage natrite (Table 8). Experimental studies showed that the maximum stability of the latter mineral is in the pH range of ~8 to 10 (Marion 2001). Based on fluid-inclusion data, as well as carbonate-carbonate and carbonate-silicate equilibria, the temperatures of late-stage fluids at Mont Saint-Hilaire are inferred to have been <400 °C (Schilling *et al.* 2011). The occurrence of steedeite and the unidentified minerals UK78 and UK80 in vugs of the same xenolith suggests that these

minerals precipitated from similar late-stage aqueous fluids. The presence of late-stage sérandite (Table 8) in the same sample as steedeite also suggests that the former mineral formed through precipitation from aqueous late-stage fluids. Both minerals occur in the same sodalite syenite boulder, but observations indicate that they are never found in the same vug together. This suggests that the aqueous fluid had localized variations in $a[\text{SiO}_4]^{4-}$ as well as $a\text{B}(\text{OH})_3$ and $a[\text{B}(\text{OH})_4]^-$, where a decrease in $a[\text{SiO}_4]^{4-}$ and an increase in $a\text{B}(\text{OH})_3$ and $a[\text{B}(\text{OH})_4]^-$ favored the development of steedeite over sérandite. A preliminary structure refinement of UK78 indicates that it also contains B, indicating that both UK78 and steedeite precipitated from similar fluids. Due to the possible variations in $a\text{BO}_3$ in the late-stage fluids, it is unclear whether or not the crystal structure of UK80 also contains B.

Another indication for the low-temperature formation of steedeite may be the conditions at which minerals of the sérandite-pectolite series form. Pectolite can be synthesized in 48 to 72 h under hydrothermal conditions with temperatures in the range of 180 to 300 °C and Ca:Si molar ratios of 0.83 (Clark & Bunn 1940, Blakeman *et al.* 1974, Xi & Glasser 1984). The existence of late-stage sérandite in the same boulder where steedeite was found implies that steedeite likely formed under a similar temperature range. It is noteworthy that steedeite represents the first mineral known to contain single looped-branched *dreier* silicate chains that may be stable over a very narrow *P–T* range. Phase-stability experiments completed on $\text{Li}_2\text{Mg}_2(\text{Si}_4\text{O}_{11})$ indicate that this phase is stable over a small pressure/temperature range: $T \sim 700\text{--}900$ °C and $P(\text{H}_2\text{O}) \sim 0\text{--}2$ kbar (Vitek & Maresch 1993). It is possible that steedeite, like $\text{Li}_2\text{Mg}_2(\text{Si}_4\text{O}_{11})$, also develops over a narrow pressure/

TABLE 8. MINERAL PARAGENESIS

Mineral	Timing
Microcline	—————
Aegirine	—————
Eudialyte	—————
Analcime	—————
Sodalite	—————
Pyrrhotite	—————
Serandite	—————
Steedeite	—————
UK78	—————
UK80	—————
Catapleite	—————
Natrite/Thermonatrite	—————

temperature range. Studies of fluid inclusions as well as associated minerals, however, indicate that steedeite likely forms at temperatures lower than Li₂Mg₂(Si₄O₁₁).

ACKNOWLEDGEMENTS

Our thanks to F.C. Hawthorne (Dept. of Geological Sciences, University of Manitoba) for providing access to the four-circle diffractometer and to Mark C. Cooper for assistance with the single-crystal XRD data collection. We also acknowledge the comments made by the two referees, Daniela Pinto and Stuart Mills, and those of the Associate Editor, Henrik Friis. Financial support this research was provided through a grant to AMM from the Natural Sciences and Engineering Research Council as well as an Alexander Graham Bell Canada Graduate Scholarship to MMMH also from the Natural Sciences and Engineering Research Council.

REFERENCES

- APPLEMAN, D.E. & CLARK, J.R. (1965) Crystal structure of reedmergnerite, a boron albite, and its relationship to feldspar crystal chemistry. *American Mineralogist* **50**, 1827–1850.
- ARAKCHEEVA, A., PATTISON, P., MEISSER, N., CHAPUIS, G., PEKOV, I., & THÉLIN, P. (2007) New insight into the pectolite – sérandite series: a single crystal diffraction study of Na(Ca_{1.73}Mn_{0.27})[HSi₃O₉] at 293 and 100 K. *Zeitschrift für Kristallographie* **222**, 696–704.
- BAKAKIN, V.V. & SOLOV'eva, L.P. (1971) Crystal structure of Fe₃BeSi₃O₉(F,OH)₂, an example of a wollastonite-like silicon-oxygen chain based on Fe. *Soviet Physics Crystallography* **15**, 999–1005.
- BLAKEMAN, E.A., GARD, J.A., RAMSAY, C.G., & TAYLOR, H.F.W. (1974) Studies on the system sodium oxide - calcium oxide - silica - water. *Journal of Chemical Technology and Biotechnology* **24**, 239–245.
- BRESE, N.E. & O'KEEFE, M. (1991) Bond-valence parameters for solids. *Acta Crystallographica* **B47**, 192–197.
- BROWN, I.D. & ALTERMATT, D. (1985) Bond-valence parameters obtained from a systematic analysis of the inorganic crystal structure database. *Acta Crystallographica* **B41**, 244–247.
- BRUGGER, J., KRIVOVICHEV, S., MEISSER, N., ANSERMET, S., & ARMBRUSTER, T. (2006) Scheuchzerite, Na(Mn,Mg)₉[VS₁₀O₂₈(OH)](OH)₃, a new single-chain silicate. *American Mineralogist* **91**, 937–943.
- CHAO, G.Y., CONLON, R.P., & VELTHUIZEN, J. (1990) Mont Saint-Hilaire Unknowns. *The Mineralogical Record* **21**, 363–368.
- CLARK, L.M. & BUNN, C.W. (1940) The scaling of boilers. Pt. IV. Identification of phases in calcium silicate scales. *Journal of the Society of Chemical Industry* **59**, 155–158.
- CROMER, D.T. & LIBERMAN, D. (1970) Relativistic calculation of anomalous scattering factors for X-rays. *Journal of Physical Chemistry* **53**, 1891–1898.
- CROMER, D.T. & MANN, J.B. (1968) X-ray scattering factors computed from numerical Hartree-Fock wave functions. *Acta Crystallographica* **A24**, 321–324.
- CZANK, M. & BISSERT, G. (1993) The crystal structure of Li₂Mg₂[Si₄O₁₁], a loop-branched dreier single chain silicate. *Zeitschrift für Kristallographie* **204**, 129–142.
- DOWTY, E. (2002) *CRYSCON for Windows and Macintosh Version 1.1*. Shape Software Kingsport, Tennessee, USA.
- FROST, R.L., BOUZAIID, J.M., MARTENS, W.N., & REDDY, J.B. (2007) Raman spectroscopy of the borosilicate mineral ferroaxinite. *Journal of Raman Spectroscopy* **38**, 135–141.
- GOBECHIYA, E.R., PEKOV, I.V., PUSHCHAROVSKÝ, D.Y., FERARIS, G., GULA, A., ZUBKOVA, N.V., & CHUKANOV, N.V. (2003) New data on vlasovite: Refinement of the crystal structure and radiation damage of the crystal during the X-ray diffraction experiment. *Crystallography Reports* **48**, 750–754.
- HAWTHORNE, F.C. (1983) Enumeration of polyhedral clusters. *Acta Crystallographica* **A39**, 724–736.
- HAWTHORNE, F.C., BURNS, P.C., & GRICE, J.D. (1996) The crystal chemistry of boron. *Reviews in Mineralogy* **33**, 41–110.
- HUANG, Y.X., EWALD, B., SCHNELLE, W., PROTS, Y., & KNIEP, R. (2006) Chirality and magnetism in a novel series of isotypic borophosphates: M^{II}[BO₄(OH)₂] (M^{II} = Mn, Fe, Co). *Inorganic Chemistry Communication* **45**, 7578–7580.
- HYBLER, J., PETŘÍČEK, V., JUREK, K., SKÁLA, R., & ČISAŘOVÁ, I. (1997) Structure determination of vistepite SnMn₄B₂Si₄O₁₆(OH)₂: Isotypism with bustamite, revised crystallographic data and composition. *Canadian Mineralogist* **35**, 1283–1292.
- JACOBSON, S.D., SMYTH, J.R., SWOPE, J.R., & SHELDON, R.I. (2000) Two proton positions in the very strong hydrogen bond of sérandite, NaMn₂[Si₃O₈(OH)]. *American Mineralogist* **85**, 745–752.
- JULIEN, C.M., MASSOT, M., & POINSIGNON, C. (2004) Lattice vibrations of manganese oxides: Part 1. Periodic structures. *Spectrochimica Acta A* **60**, 689–700.
- LIEBAU, F. (1978) Silicates with branched anions: a crystallochemically distinct class. *American Mineralogist* **63**, 918–923.
- MANDARINO, J.A. (1981) The Gladstone-Dale relationship: Part IV. The compatibility concept and its application. *Canadian Mineralogist*. **19**, 441–450.
- MARESCH, W.V. & CZANK, M. (1985) The optical and X-ray properties of Li₂Mg₂[Si₄O₁₁], a new type of chain-silicate. *Neues Jahrbuch für Mineralogie* **7**, 289–297.

- MARION, G.M. (2001) Carbonate mineral solubility at low temperatures in the Na-K-Mg-Ca-H-Cl-SO₄-OH-HCO₃-CO₂-CO₂-H₂O system. *Geochimica et Cosmochimica Acta* **65**, 1883–1896.
- MASON, R. A. (1980) Changes in crystal morphology of synthetic reedmergnerite (NaBSi₃O₈) during ordering experiments. *Mineralogical Magazine* **43**, 905–908.
- MCDONALD, A.M. & CHAO, G.Y. (2005) Bobtraillite, (Na,Ca)₁₃Sr₁(Zr,Y,Nb)₁₄Si₄₂B₆O₁₃₂(OH)₁₂•12H₂O a new mineral species from Mont Saint-Hilaire, Québec: description, structure determination and relationship to benitoite and wadeite. *Canadian Mineralogist* **43**, 747–758.
- MCDONALD, A.M. & CHAO, G.Y. (2009) Lalondeite, a new hydrated Na-Ca fluorosilicate species from Mon Saint-Hilaire, Québec: Description and crystal structure. *Canadian Mineralogist* **47**, 181–191.
- MCDONALD, A.M. & CHAO, G.Y. (2010) Rogermitchellite, Na₁₂(Sr,Na)₂₄Ba₄Zr₂₆Si₇₈(B,Si)₁₂O₂₄₆(OH)₂₄•18H₂O, a new mineral species from Mont Saint-Hilaire, Québec: description, structure determination and relationship with HFSE-bearing cyclosilicates. *Canadian Mineralogist* **48**, 267–278.
- PREWITT, C.T. (1967) Refinement of the crystal structure of pectolite, Ca₂NaHSi₃O₉. *Zeitschrift für Kristallographie* **125**, 298–316.
- ROZHDESTVENSKAYA, I., MUGNAIOLI, E., CZANK, M., DEPMEIER, W., KOLB, U., REINHOLDT, A., & WEIRICH, T. (2010) The structure of charoite, (K,Sr,Ba,Mn)₁₅₋₁₆(Ca,Na)₃₂[(Si₇₀(O,OH)₁₈₀](OH,F)_{4,0}•nH₂O, solved by conventional and automated electron diffraction. *Mineralogical Magazine* **74**, 159–177.
- SCHILLING, J., MARKS, M.A.W., WENZEL, T., VENNEMANN, T., HORVATH, L., TARASSOFF, P., JACOB, D.E., & MARKL, G. (2011) Magmatic to hydrothermal evolution of the intrusive Mont Saint-Hilaire complex: insights into the late-stage evolution of peralkaline rocks. *Journal of Petrology* **52**, 2147–2185.
- SHANNON, R.D. (1976) Revised effective ionic radii and systematic studies in interatomic distances in halides and chalcogenides. *Acta Crystallographica* **A32**, 751–767.
- SHELDRIK, G.M. (1997) *SHELXL-97: A computer program for the Refinement of Crystal Structures*. University of Göttingen, Göttingen, Germany.
- SHELDRIK, G.M. (1998) *SADABS*. University of Göttingen, Göttingen, Germany.
- SHELDRIK, G.M. (2008) A short history of *SHELX*. *Acta Crystallographica* **A64**, 112–122.
- SOKOLOVA, E., HAWTHORNE, F.C., BALL, N.A., & MITCHELL, R.H. (2006) Vlasovite, Na₂Zr(Si₄O₁₁), from the Kipawa alkaline complex, Québec, Canada: crystal-structure refinement and infrared spectroscopy. *Canadian Mineralogist* **44**, 1349–1356.
- THOMPSON, J.B. (1970) Geometrical possibilities for amphibole structures: Model biopyriboles. *American Mineralogist* **63**, 239–249.
- VILLARS, P., CENZUAL, K., DAAMS, J., GLADYSHEVSKII, R., SHCHERBAN, O., DUBENSKYY, V., KUPRYSYUK, V., & SAVYSYUK, I. (2010) Pb₆B₁₁O₁₈(OH)₉. *Crystal Structures of Inorganic Compounds* **43A9**, 501–502.
- VITEK, E. & MARESC, W.V. (1993) Synthesis and stability regions of Li₂Mg₂[Si₄O₁₁]. *European Journal of Mineralogy* **5**, 1121–1131.
- VORONKOV, A.A. & PYATENKO, Y.A. (1962) The crystal structure of vlasovite. *Soviet Physics Crystallography* **6**, 755–760.
- WALDEMARW, T.S. (1955) The pectolite-serandite series. *American Mineralogist* **40**, 1022–1031.
- WILLIAMS, Q. (1995) Infrared, Raman and optical spectroscopy of Earth materials. In *Mineral Physics and Crystallography: A Handbook of Physical Constants* (T.J. Ahrens, ed.). American Geophysical Union, Washington, D.C., U.S.A. (291–302).
- XI, Y. & GLASSER, L.S.D. (1984) Hydrothermal study in the system Na₂O-CaO-SiO₂-H₂O at 300 degrees Celsius. *Cement Concrete Research*, **14**, 741–748.

Received October 22, 2013, revised manuscript accepted February 21.